Applied Catalysis B: Environmental 198 (2016) 67–73

Contents lists available at ScienceDirect

Applied Catalysis B: Environmental

journal homepage: www.elsevier.com/locate/apcatb

Photocatalytic hydrogen evolution based on Cu_2ZnSnS_4, Cu_2NiSnS_4 and Cu_2CoSnS_4 nanocrystals

Faruk Ozel [a,*], Emre Aslan [b], Bilal Istanbullu [c], Ozge Akay [c], Imren Hatay Patir [b,*]

[a] Department of Metallurgical and Materials Engineering, Karamanoglu Mehmetbey University, 70200, Karaman, Turkey
[b] Department of Chemistry, Selcuk University, Konya 42130, Turkey
[c] Department of Nanotechnology and Advanced Materials, Selcuk University, 42030 Konya, Turkey

ARTICLE INFO

Article history:
Received 26 January 2016
Received in revised form 5 May 2016
Accepted 21 May 2016
Available online 24 May 2016

Keywords:
Nanocrystals
Hydrogen evolution
Cu_2ZnSnS_4
Cu_2CoSnS_4
Cu_2NiSnS_4

ABSTRACT

A low cost and environment-friendly Cu_2ZnSnS_4, Cu_2CoSnS_4 and Cu_2NiSnS_4 nanocrystals have been used as a catalyst instead of noble metal Pt for the photocatalytic hydrogen evolution in the presence of triethanolamine and eosin Y as a sacrificial reducing agent and a photosensitizer, respectively under visible light irradiation. Cu_2NiSnS_4 and Cu_2CoSnS_4 nanocrystals exhibit a longer photostability and a higher hydrogen evolution rate of 1200 $\mu molg^{-1}\ h^{-1}$, 900 $\mu molg^{-1}\ h^{-1}$, respectively, compared to that of Cu_2ZnSnS_4 by producing hydrogen 670 $\mu molg^{-1}\ h^{-1}$.

1. Introduction

Solar water splitting for hydrogen production has drawn tremendous global interests for the efficient evolution of clean hydrogen, which offers a promising solution to the growing energy crisis and the environmental problems. Until now, many photocatalytic hydrogen evolution systems, which usually consist of a photosensitizer, a sacrificial electron donor and catalysts, have been reported to have low-cost and high photocatalytic activity under visible light irradiation. Therefore, the development of photocatalytic systems based on cheap and noble-metal free catalysts has attracted interest of a large number of researchers. Copper-based quaternary chalcogenides of earth-abundant elements have recently emerged as promising alternative materials for solar energy conversion due to their outstanding photovoltaic and photocatalytic properties [1]. A quaternary chalcogenide semiconductor Cu_2ZnSnS_4 (CZTS) have been intensively explored for the photoelectrochemical water splitting due to its high absorbtion (>10^4 cm^{-1}), abundance and nontoxicity [2–8]. Recently, CZTS nanocrystals [9], CZTS nanosheets [10], CZTS-Pt, CZTS-Au heterostructured nanoparticles [11], CZTS nanorod, CZTS nanoplate and Au/CZTS core/shell nanoparticles [12] have been studied in the photocatalytic water splitting system in the presence of Na_2S/Na_2SO_3 as hole scavengers. The high electrocatalytic activity for the oxygen and hydrogen evolution reactions has been also reported by using CZTS nanoparticles [13]. In addition, more recently, the photocatalytic hydrogen evolution activity of eosin (EY) dye sensitized CZTS, $Cu_2ZnSnSe_4$ (CZTSe), $Cu_2ZnSnSe_{4-x}S_x$ (CZTSeS), Cu_2NiSnS_4 (CNTS), Cu_2FeSnS_4 (CFTS), Cu_2CoSnS_4 (CCTS) and Cu_2MnSnS_4 (CMTS) nanofibers has been firstly reported by our group in the presence of triethanolamine (TEOA) as a sacrificial electron donor under visible-light irradiation ($\lambda > 420$ nm) [14,15]. Compared with CZTS, CZTS-like compounds such as Cu_2CoSnS_4 (CCTS), Cu_2NiSnS_4 (CNTS), have not been extensively studied applications in water splitting catalysis, despite having good potential as another low-cost and eco-friendly materials. Ha et al. have been reported in 2015 that Au/Cu_2FeSnS_4 core/shell nanostructures show photocatalytic activity for hydrogen generation [16]. We have also shown that CCTS nanofibers display highly comparable rates of catalysis to Pt particles for the electrocatalytic hydrogen evolution by using decamethylferrocene as an electron donor at water-1,2dichloroethane (DCE) interfaces [17].

Herein, we report, for the first time, an efficient photocatalytic system for hydrogen evolution reaction (HER) by using CCTS and

* Corresponding authors.
E-mail addresses: farukozell@gmail.com (F. Ozel), imrenhatay@gmail.com (I. Hatay Patir).

http://dx.doi.org/10.1016/j.apcatb.2016.05.053
0926-3373/

CNTS nanocrystals as the catalyst, an organic dye EY as the photosensitizer and TEOA as a sacrificial agent under visible light irradiation. The catalytic effect of these nanocrystals in this system has been also compared to that of CZTS nanocrystals and Pt. These results open the possibility of engineering new generation of nanocrystals as noble metal alternative catalysts for H_2 production.

2. Experimental

2.1. Materials

Copper(II) acetate ($Cu(CO_2CH_3)_2$), Zinc acetate ($((CH_3CO_2)_2Zn$), Cobalt(II) acetate ($((CH_3CO_2)_2Co$), Nickel(II) acetate tetrahydrate ($Ni(OCOCH_3)_2{\cdot}4H_2O$), Sulfur powder, Ethanol and EY were obtained from Sigma-Aldrich. Tin(II) acetate $Sn(OOCCH_3)_2$ and TEOA were purchased from Alfa Aesar. Oleylamine – % 80–90 (OLA) was obtained from Across organic. Toluene and 2-Propanol were obtained from VWR. Hydrochloric acid (HCl, 37.5%) and sodium hydroxide (NaOH) were attained from Merck.

2.2. Instrumentation

X-ray diffraction (XRD) patterns of CZTS, CCTS and CNTS nanoparticles were obtained on a Bruker D8 Advance with Cu-Kα radiation source (λ = 0.15406 Å). Zeiss Evo model scanning electron microscope was used for analyzing of atomic percentage of elements. The microscopic images and selected area electron diffraction pattern (SAED) of samples were recorded by a transmission electron microscope (TEM, JEOL JEM-2100). The optical properties of the nanocrystals were measured in a wide spectral range from 200 to 2500 nm by UV-VIS-NIR spectrophotometer (Jasco V-670 photospectrometer). Solar Light – XPS 300TM was used as the visible light source. The amount of evolved hydrogen was analyzed using a gas chromatograph (Shimadzu GC-2010 Plus, detector, TCD; column temperature, 323 K; column, RESTEK molecular sieve 5A porous layer open tubular capillary column 30 m 0.53 mm ID 50 μm df; Ar as a carrier gas) and calculated by calibration using standard samples of hydrogen in nitrogen.

2.3. The synthesis of CZTS, CNTS and CCTS nanocrystals

The Synthesis of CZTS, CCTS and CNTS nanocrystals was carried out based on previously published hot-injection process by using metal salts and oleylamine precursors as starting materials and capping agent, respectively [18,19]. Typically; 1 mmol $Cu(CO_2CH_3)_2$, 0.5 mmol M(II) acetate (M = Zn, Co, Ni) were added separately, depending upon the desired chemical structure, 0.5 mmol$Sn(OOCCH_3)_2$ and 20 mL OLA were added to a 25 mL two-neck flask and heated to 280 °C under N_2 flow. Following the colors changes from blue to reddish brown, a solution of sulfur in oleylamine was added to above solution. Then, the temperature is increased to 280 °C and kept for 30 min by stirring. After cooling down to the room temperature, the resultants were participated and centrifuged. The final product was washed with ethanol and dried at 70 °C.

2.4. Optical and electrochemical characterization of CZTS, CNTS and CCTS nanocrystals

The room temperature UV–vis-NIR absorption spectra of the nanocrystals were performed by dispersing samples in toluene as 0.1 mg/mL concentration. Electrochemical characterizations of the nanocrystals were carried out by cyclic voltammetry technique. The glassy carbon electrode, Pt electrode and Ag/AgCl electrode was used to perform electrochemical measurements as a working electrode, counter electrode and reference electrode, respectively. All potentials were reported versus the Ag/AgCl (+0.211 V vs. SHE) [20]. Tetrabutylammonium hexafluorophosphate in acetonitrile was used as the supporting electrolyte under N_2 atmosphere.

2.5. Photocatalytic hydrogen evolution by using CZTS, CNTS and CCTS nanocrystals

Photocatalytic experiments were performed in the quartz glass flask with the total volume 135 mL under solar simulator at room temperature (25 ± 2 °C). TEOA (0.33 M) and EY (0.33 mM) solutions were bubbled with N_2 to remove O_2 and taken into the glove box. A total volume of solution 20 mL TEOA, EY and nanocrystals (CZTS, CNTS or CCTS, 10 mg) were taken into the photo-reaction glass flasks. The reaction flask was sealed tightly with a rubber

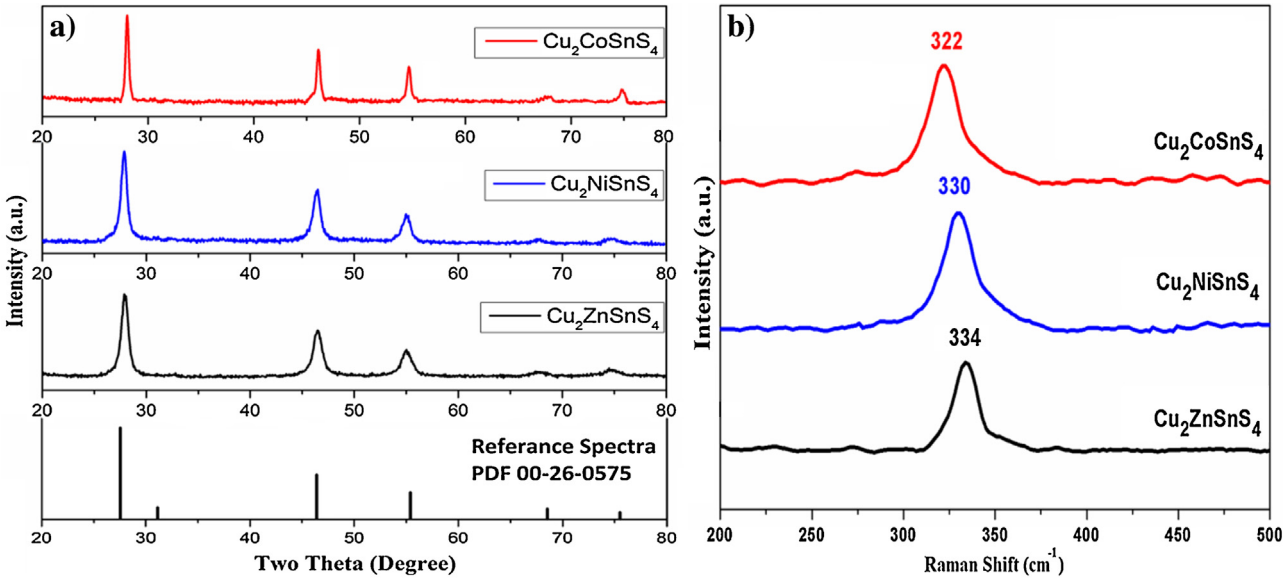

Fig. 1. (a) X-Ray Diffraction (XRD) and (b) Raman results for CZTS (black line), CNTS (blue line) and CCTS (red line) nanocrystals. (For interpretation of the references to colour in this figure legend, the reader is referred to the web version of this article.)

septum and stirred vigorously under the visible light source. The amount of hydrogen in the headspace was measured by gas chromatography. After this process, some experiments were performed for reusability of catalyst in the same condition. Catalyst-electron donor-sensitizer mixture was centrifuged and CZTS, CCTS and CNTS catalysts were reused in the same conditions for reusability of catalyst.

3. Results and discussion

3.1. Characterization of nanocrystals

The crystal structure of CZTS, CCTS and CNTS nanocrystals has been investigated by X-ray diffraction (XRD) analysis and the results are presented in Fig. 1a. Characteristic peaks of nanocrystals are clearly observed on the diffraction patterns. All of the synthesized nanocrystals showed three intensive XRD peaks centered at $2\theta = \sim 28^\circ$, $\sim 47^\circ$ and $\sim 56^\circ$ corresponding planes to (112), (220) and (312), respectively. The nanocrystals can be regarded as deriving from the tetragonal structure of ZnS, CoS and NiS, in which there are eight atoms per primitive cell with a body-centered tetragonal symmetry [21]. In this phase; sulfur and cations are arranged in crystallographic c-direction, since sulfur ions are joined to four cations, which are joined to four anions [22]. Since their same crystal structure, CZTS, CCTS and CNTS nanocrystals show similar patterns.

Displacement of the Co and Ni atoms with Zn atoms in the lattice structure does not cause any change in tetragonal arrangement [23]. As well known, XRD peaks are broadened by decreasing the particle size. The sample of nanocrystals shows broad diffraction peaks and these broad peaks are due to the small size of the CZTS, CCTS and CNTS nanocrystals. The average particle size of the nanocrystals were calculated from the (112) diffraction peaks at ~280 by using Debye-Sherrer equation as 19 ± 2 nm, which is also confirmed by TEM analysis.

The phase purity of the nanocrystals was further studied by Raman analysis. As shown in Fig. 1b, the characteristic Raman peak at 334 corresponded to the A_1 modes of kesterite phase of CZTS [21,24]. However, the CNTS and CCTS appeared to shift to the lower frequency direction compared with the CZTS peak positions. These similar vibration modes independent from mass effects and they are originated from the only sulfur atoms. Consequently the dominant peak at higher frequencies shows a certain dependence on the Ni—S, Co—S and Zn—S force constants [25]. Moreover; no raman peaks associated with other crystalline forms were detected, which demonstrates that all of the samples had high purity and crystallinity.

The overall composition of CZTS, CNTS and CCTS nanocrystals was analyzed by Energy-dispersive spectroscopy (EDAX) (Fig. 2). The average elemental composition ratio of CZTS, CNTS and CCTS nanocrystals were found as $Cu_2Zn_{0.9}Sn_1S_4$, $Cu_2Ni_{0.9}Sn_1S_4$ and $Cu_2Co_1Sn_1S_4$, respectively, which are revealed that all sample close to the theoretical value of 2:1:1:4.

Fig. 3 shows the TEM images and SAED patterns of the CZTS, CCTS and CNTS nanocrystals. As can be clearly seen from Fig. 3(a, c and e), most of the nanocrystals are triangular and spherical with an average diameter of 18 ± 5 nm. To further study crystallinity and confirm the structure of the nanocrystals, HR-TEM analysis was carried out. The lower right inset in Fig. 3(a, c and e) gives HR-TEM images of the nanocrystals, all of the lattice fringes of the nanocrystals revealed the highly crystalline nature. Moreover, interplanar spacing of ~3.1 Å was measured and attributed to the (112) crystallographic planes. Fig. 3(b, d and f) gives a SAED pattern of the nanocrystals, in which three main diffraction rings correspond to (112), (220) and (312) planes of polycrystalline CZTS, CCTS and CNTS nanocrystals with tetragonal structure [21–23]. Furthermore, as shown in Fig. 3(b, d and f), the diffraction rings are discontinuous and consist of sharp spots, which indicate that the nanocrystals are well crystallized.

Fig. 4 shows the room temperature UV–vis absorption spectra of the CZTS, CCTS and CNTS nanocrystals. As can be clearly seen from Fig. 4, all of the nanocrystal samples exhibited strong and broad absorption in the UV region and the tails extending to red region. The optical band gap value, as shown in the inset of Fig. 4, determined by plotting $(Ah\upsilon)^2$ versus $h\upsilon$ and extrapolating the linear portion of the spectrum in the band edge region. The optical band gaps of CZTS, CCTS and CNTS nanocrystals were measured at around 1.59, 1.18 and 1.45 eV, respectively. Note that these band gaps are in the range of 1.1–1.6 eV depending on the elemental content of structures. The measured band gaps are shift from bulk CZTS materials (1,4–1,5 eV) [26]. The possible reason for this shift is the quantum confinement effect and composition variation of the nanostructure the samples [26,27]. Also, the obtained band gap value is close to the optimal values reported in the literature for solar cell applications [19,27–30].

Electrochemical conduction band (CB) energy levels of nanocrystals were calculated from the first reduction peak potentials. CB of CNTS, CCTS and CZTS nanocrystals were found out −0.88 V, −0.83 V and −0.65 V, respectively (Fig. 5). The energy lev-

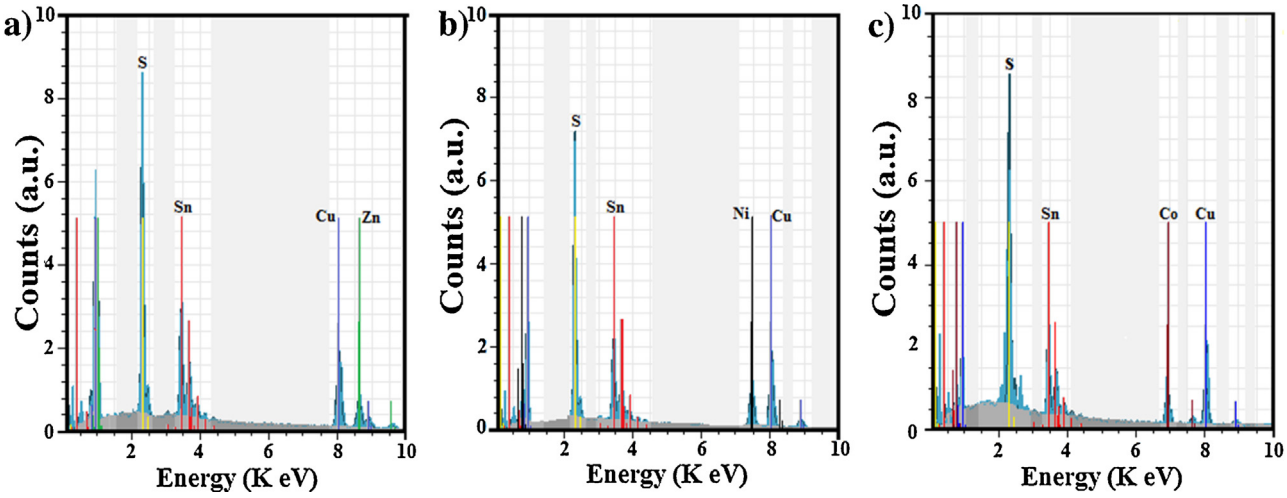

Fig. 2. EDAX spectrums of CZTS (a), CNTS (b) and CCTS (c) nanocrystals.

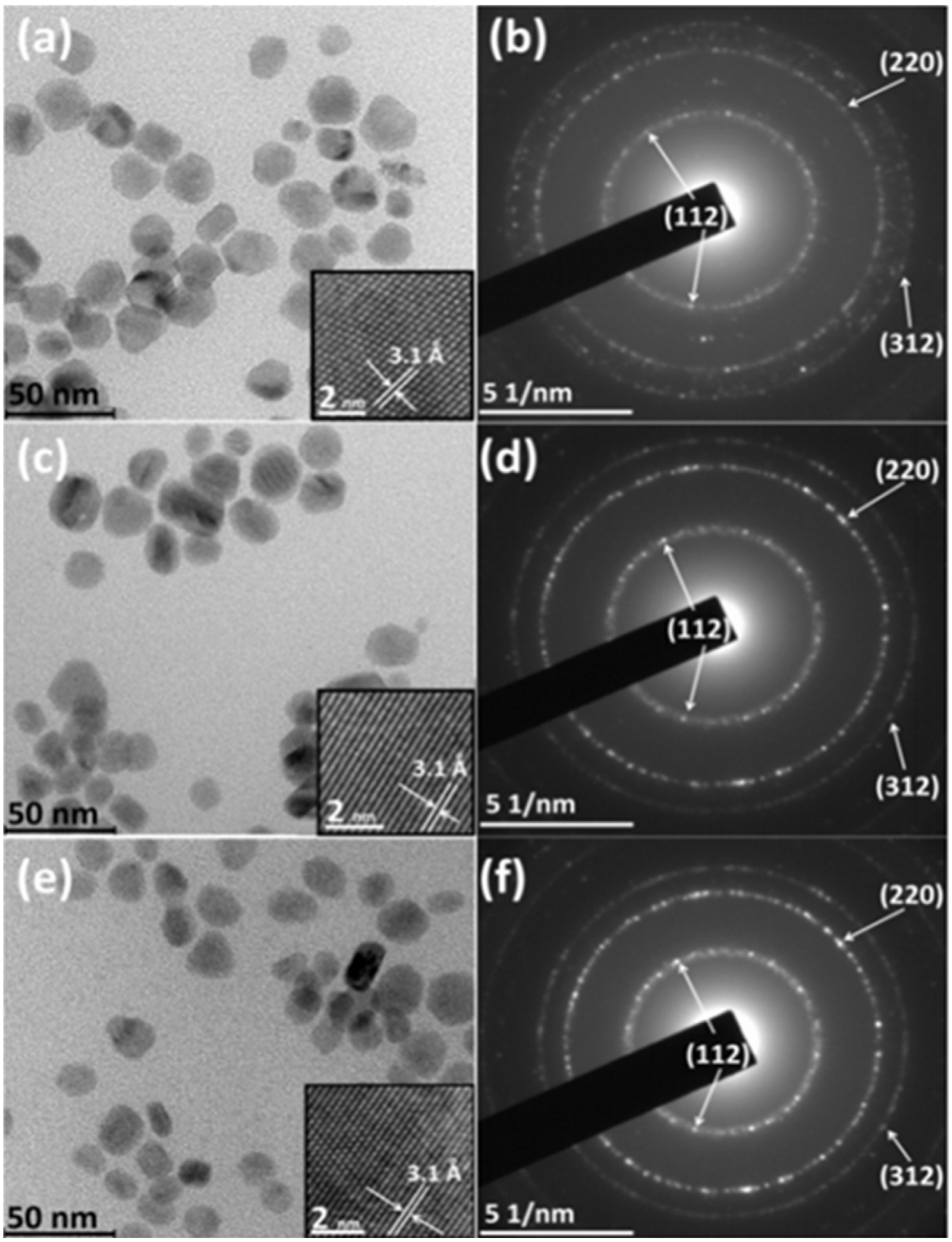

Fig. 3. (a, c, e) shows TEM images, lower right inset in figure (a, c, e) shows the HR-TEM images and figure (b, d, f) shows SAED patterns of CZTS, CCTS, CNTS nanocrystals, respectively.

els versus vacuum level were calculated according to the following equation.

$$E_{LUMO} = -e(E_{onset.red} + 4.75)$$

LUMO energy levels of CNTS, CCTS and CZTS were calculated −3.87 eV, −3.92 eV and −4.1 eV respectively. Subsequently, band gaps of CNTS, CCTS and CZTS nanocrystals were determined by UV–vis-NIR data 1.45, 1.18 and 1.59 eV respectively. Valance band (VB) energy levels were found out by subtracting CB energy levels from optical band gaps. VB energy levels of CNTS, CCTS and CZTS nanocrystals were −5.32 eV, −5.1 eV and 5.69 eV, respectively (energy band diagrams of CZTS, CNTS and CCTS nanocrystals are shown in Fig. S1).

3.2. The photocatalytic hydrogen evolution by Cu_2ZnSnS_4, Cu_2NiSnS_4 and Cu_2CoSnS_4 nanocrystals

The photocatalytic activities of CNTS, CCTS and CZTS nanocrystals for the HER were investigated under visible light irradiation (≥420 nm) using EY dye as a photosensitizer and TEOA as a sacrificial electron donor. No hydrogen gas was detected in the absence of any one of them (eosin Y, TEOA and nanocrystals). First of all, the photocatalytic HER was investigated with the system of TEOA, EY and nanocrystals (CZTS, CCTS or CNTS) under different pH values from 7 to 10 for 1 h irradiation of visible light as shown in Fig. 6.

The pH value of the solution showed notable effect on the photocatalytic activity as discussed in our earlier studies [14,15]. The highest rate of hydrogen production was achieved at pH 9 and the rates of hydrogen evolution were detected to be 1200, 900,

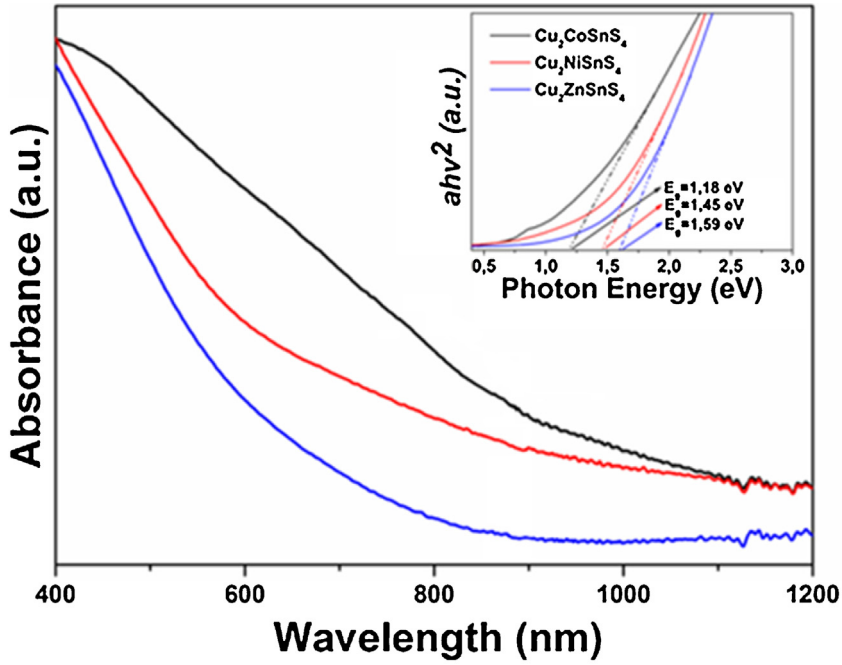

Fig. 4. UV–vis absorption spectrums, inset show the calculated eV diagrams of CZTS (blue line), CCTS (black line) and CNTS (red line) nanocrystals. (For interpretation of the references to colour in this figure legend, the reader is referred to the web version of this article.)

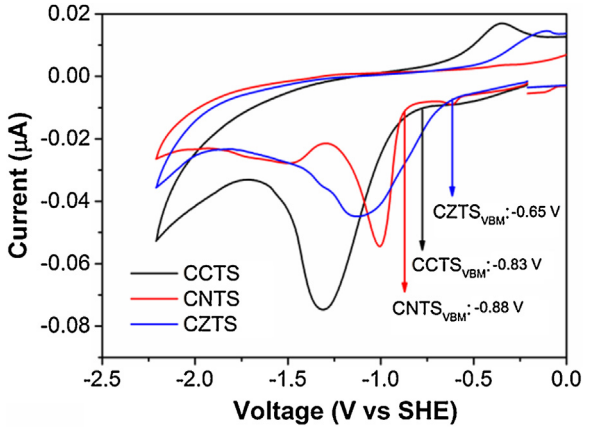

Fig. 5. Cyclic voltammograms of CZTS (blue line), CCTS (black line) and CNTS (red line) nanocrystals (Scan rate: 100 mV s^{-1}, tetrabutylammonium hexafluorophosphate in acetonitrile as the support electrolyte). (For interpretation of the references to colour in this figure legend, the reader is referred to the web version of this article.)

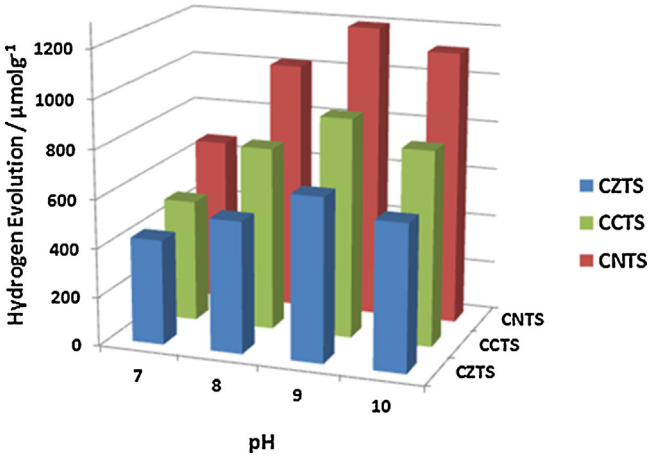

Fig. 6. Effect of pH on the photocatalytic H_2 evolution activity from the system comprising CZTS, CCTS and CNTS nanocrystals (10 mg), EY (3.25×10^{-4} M), and TEOA an electron donor (0.33 M) in H_2O over 1 h irradiation.

670 μmol g^{-1} h^{-1} using CNTS, CCTS and CZTS nanocrystals as the catalyst. When the pH is more acidic, the significant decrease of hydrogen evolution likely results from protonation of TEOA, which might render TEOA an ineffective sacrificial donor. When the pH is more basic, the driving force for hydrogen generation is decreased (the redox potential of H^+/H_2 will become more negative at high pH value). This pH dependence for many hydrogen evolution systems is a common phenomenon [31–33].

Fig. 7a shows time course of photocatalytic hydrogen evolution catalyzed by the EY dye sensitized CNTS, CCTS and CZTS nanocrystal catalysts in TEOA aqueous solution at pH 9 under visible light irradiation. CNTS and CCTS nanocrystals exhibit a higher hydrogen evolution rate of 1200 μmol g^{-1} h^{-1}, 900 μmol g^{-1} h^{-1}, respectively compared to that of CZTS by producing hydrogen 670 μmol g^{-1} h^{-1}. When a sample of CNTS, CCTS or CZTS nanocrystals is irradiated in TEOA-EY reaction system at pH 9 for 8 h, they produce a total of 9.2, 6.2 and 1.3 mmol g^{-1} of H_2, respectively. In addition, reusability experiment were carried out with the CZTS, CCTS and CNTS catalysts in the same conditions and they were almost displayed the same catalytic activity (Fig. 7b). Moreover, the photocatalytic hydrogen evolution activity of nanocrystals has been also compered to that of Pt under the same conditions with nanocrystals. As shown in Fig. 6a, the hydrogen production rate in the system of TEOA-EY-Pt is higher than nanocrystals in the first two hours but ceases after two hours. Also, CZTS nanocrystal, which shows less catalytic activity than Pt during 8 h photocatalytic reaction, is also follow the similar trend with Pt. However, CNTS and CCTS nanocrystals exhibit a good photostability in the

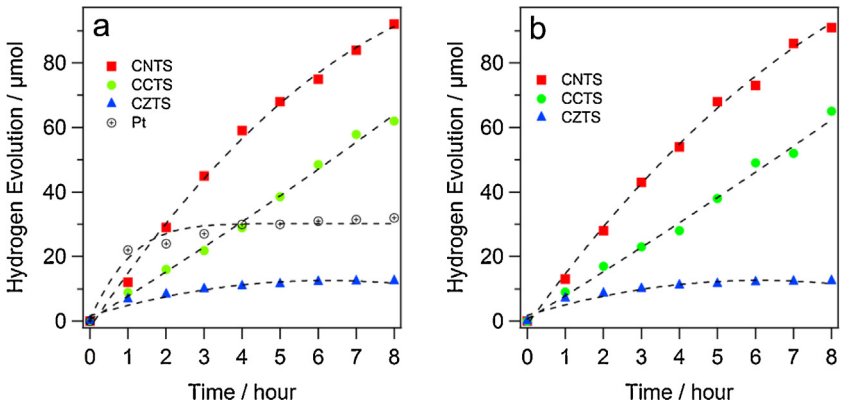

Fig. 7. Hydrogen evolution with time in the system composed of CZTS, CCTS and CNTS nanocrystals (10 mg) or Pt catalysts in the presence of EY (3.25×10^{-4} M) and TEOA (0.33 M) in 20 mL H_2O at pH = 9 (a) and reusability results of CZTS, CCTS and CNTS nanocrystals in the same conditions (b).

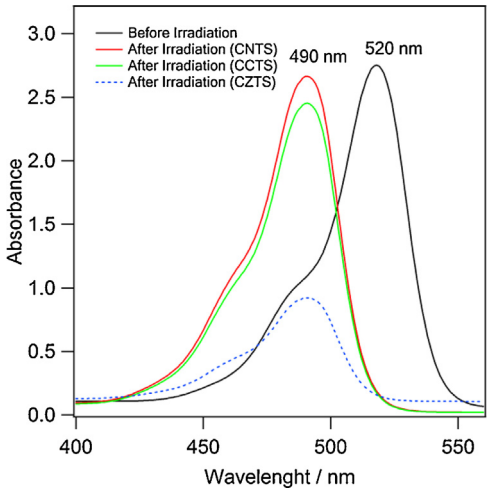

Fig. 8. UV–vis absoption spectra of the solutions before and after photocatalytic hydrogen evolution system containing 10 mg CZTS, CCTS or CNTS, Eosin Y (3.25×10^{-4} M) and TEOA (0.33 M) in 20 mL H_2O at pH = 9.

hydrogen evolution more than 8 h under visible light irradiation. The photostability difference of CNTS, CCTS or CZTS nanocrystal catalysts might be attributed to the degradation behaviors of EY.

This behavior is also supported by UV–vis absorption spectra. As shown in Fig. 8, the strong characteristic absorption peak at 520 nm for EY before irradiation shifts to about 490 nm. This shift can be also assigned to that some bromides of EY were removed and fluorescein-like species might be formed [34,35]. The intensity of absorption peak gradually weakened after irradiation of TEOA-EY-CZTS nanocrystal system by visible light for 8 h, which indicates that the sensitizer EY may be almost completely degraded during the reaction [13,36]. Kush et al. have been reported that the CZTS nanoparticle catalysts have also applications in polluting dye degradation reactions [13]. However, the intensity decrease of absorption peak by using CNTS and CCTS nanocrystals is lower than that of CZTS. This result indicated that CNTS and CCTS nanocrystals could efficiently reduce the degradation rate of EY under visible light irradiation for 8 h, producing more hydrogen comparing to that of CZTS.

The mechanism of photocatalytic hydrogen evolution is illustrated in Fig. 9. EY (E_{ox} = 0.89 V vs. standard hydrogen electrode (SHE) [37]) can absorb light to generate the excited state of *EY (−1.1 V [38]). Electrons liberated from *EY are transferred to the CB of CNTS, CCTS and CZTS nanocrystals, −0.88 V, −0.83 V,−0.65 V (see Fig. 5 for the cyclic voltammetry measurements) for the HER (nanocrystals act role as an electron acceptor). This reaction take place easily due to the more negative CB levels of the nanocrystals than the reduction potential of proton to hydrogen (−0.53 vs. NHE at pH 9) [39]. The difference between hydrogen evolutions activity of CNTS, CCTS and CZTS nanocrystals may not be attributed to the energy levels. More recently, Yu et al. have been reported that Cu_2ZnSnS_4-PtM (M = Co, Ni) nanoheterostructures showed a higher photocatalytic activities toward hydrogen evolution from water when compared to both the bare CZTS and the CZTS-Pt [40]. Herein, the higher activity was ascribed to the enhanced charge carrier separation and transport efficiency, which are two of the key parameters in the photocatalytic hydrogen production. The presence of Co increased the accumulation of photoexcited electrons in the nanocrystals and facilitated the charge transfer to the surface adsorbed species such as proton. Therefore, we suggest that the similar approach may be also valid for the hydrogen evolution activity differences of CNTS, CCTS and CZTS nanocrystals.

More recently, the catalytic effect of CXTS (X = Zn, Ni, Fe, Co and Mn) nanofibers on the photocatalytic hydrogen evolution is also investigated under the same conditions with nanocrystals used in this work [15]. CNTS, CCTS and CZTS nanofibers show about two times higher hydrogen evolution rate of 2028, 1926, and 1420 $\mu mol\, g^{-1}\, h^{-1}$, respectively compared to that of CNTS, CCTS and CZTS nanocrystals. This may be attributed that charge transport efficiency in the hydrogen evolution reactions and photovoltaic devices are enhanced by using 1-D semiconductors such as nanowires [41], nanofibers [39,42,43] and nanotubes [43].

4. Conclusion

To conclude, three types of quaternary CNTS, CCTS or CZTS semiconductor nanocrystals have been firstly investigated for the dye sensitized photocatalytic hydrogen evolution. It has been found that CNTS and CCTS nanocrystals serve as a highly efficient and stable catalysts as an alternative to noble metals (such as Pt) for hydrogen evolution from water under visible light irradiation. Thus we may suggest that such catalysts, made of inexpensive and abundant materials hold great promise for a variety of applications in the fields of energy conversion systems.

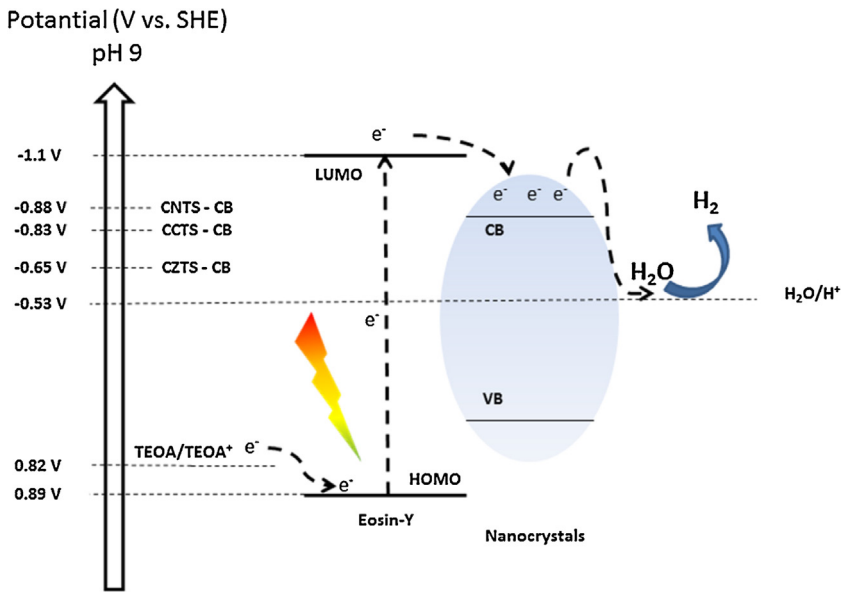

Fig. 9. Proposed mechanism for photocatalytic hydrogen evolution over EY sensitized nanocrystals.

Conflict of interest

The authors declare no competing financial interest.

Acknowledgments

The authors would like to thank TUBITAK (The Scientific and Technological Research Council of Turkey) (211T185 and 214M366), the COST Action (MP1106), Selcuk University and Karamanoglu Mehmetbey University, Scientific Research Council for supporting this work.

Appendix A. Supplementary data

Supplementary data associated with this article can be found, in the online version, at http://dx.doi.org/10.1016/j.apcatb.2016.05.053.

References

[1] D. Aldakov, A. Lefrancois, P. Reiss, J. Mater. Chem. C 1 (2013) 3756–3776.
[2] D. Yokoyama, T. Minegishi, K. Jimbo, T. Hisatomi, G. Ma, M. Katayama, J. Kubota, H. Katagiri, K. Domen, Appl. Phys. Express 3 (2010) 101202.
[3] X. Wen, W. Luo, Z. Zou, J. Mater. Chem. A 1 (2013) 15479–15485.
[4] L. Rovelli, S.D. Tilley, K. Sivula, ACS Appl. Mater. Interfaces 5 (2013) 8018–8024.
[5] E. Ha, L.Y.S. Lee, J. Wang, F. Li, K.-Y. Wong, S.C.E. Tsang, Adv. Mater. 26 (2014) 3496.
[6] G. Ma, T. Minegishi, D. Yokoyama, J. Kubota, K. Domen, Chem. Phys. Lett. 501 (2011) 619–622.
[7] Z. Guan, W. Luo, Z. Zou, Cryst. Eng. Comm. 16 (2014) 2929–2936.
[8] B. Li, P. Yin, Y. Zhou, Z. Gao, T. Ling, X. Du, RSC Adv. 5 (2015) 2543.
[9] J. Wang, P. Zhang, X. Song, L. Gao, RSC Adv. 4 (2014) 27805–27810.
[10] L. Wang, W. Wang, S. Sun, J. Mater. Chem. 22 (2012) 6553–6555.
[11] X. Yu, A. Shavel, X. An, Z. Luo, M. Ibanez, A. Cabot, J. Am. Chem. Soc. 136 (2014) 9236–9239.
[12] E. Ha, L.Y.S. Lee, J. Wang, F. Li, K. Wong, S.C.E. Tsang, Adv. Mater. 26 (2014) 3496–3500.
[13] P. Kush, K. Deori, A. Kumar, S. Deka, J. Mater. Chem. A 3 (2015) 8098–8106.
[14] M.K. Gonce, M. Dogru, E. Aslan, F. Ozel, I.H. Patir, M. Kus, M. Ersoz, RSC Adv. 5 (2015) 94025–94028.
[15] M.K. Gonce, E. Aslan, F. Ozel, I. Hatay Patir, ChemSusChem 9 (2016) 600–605, http://dx.doi.org/10.1002/cssc.201501661.
[16] E. Ha, L.Y.S. Lee, H. Man, S.C.E. Tsang, K. Wong, ACS Appl. Mater. Interfaces 7 (2015) 9072–9077.
[17] F. Ozel, A. Yar, E. Aslan, E. Arkan, A. Aljabour, M. Can, I.H. Patir, M. Kus, M. Ersoz, ChemNanoMat 1 (2015) 477.
[18] S.C. Riha, B.A. Parkinson, A.L. Prieto, J. Am. Chem. Soc. 131 (2009) 12054–12055.
[19] M. Kuş, F. Özel, S. Büyükçelebi, A. Aljabour, A. Erdoğan, M. Ersöz, N.S. Sariçiftci, Opt. Mater. 39 (2015) 103–109.
[20] J. Gasiorowskia, A.I. Mardareb, N.S. Sariciftci, A.W. Hasser, Electrochim. Acta 113 (2013) 834–839.
[21] C. Huang, Y. Chan, F. Liu, D. Tang, J. Yang, Y. Lai, J. Lia, Y. Liu, J. Mater. Chem. A 1 (2013) 5402–5407.
[22] C. Yan, C. Huang, J. Yang, F. Liu, J. Liu, Y. Lai, J. Li, Y. Liu, Chem. Commun. 48 (2012) 2603–2605.
[23] F. Ozel, J. Alloys Compd. 657 (2016) 157–162.
[24] J. He, L. Sun, S. Chen, Y. Chen, P. Yang, J. Chu, J. Alloys Compd. 511 (2012) 129–132.
[25] X. Fontane, V. Izquierdo-Roca, E. Saucedo, S. Schorr, V.O. Yukhymchuk, M.Y. Valakh, A. Perez-Rodriguez, J.R. Morante, J. Alloys Compd. 539 (2012) 190–194.
[26] Z. Su, C. Yan, D. Tang, K. Sun, Z. Han, F. Liu, Y. Lai, J. Li, Y. Liu, Cryst. Eng. Commun. 14 (2012) 782.
[27] A. Gillorin, A. Balocchi, X. Marie, P. Dufoura, J.Y. Chane-Ching, J. Mater. Chem. 21 (2011) 5615.
[28] Y. Cui, R. Deng, G. Wang, D. Pan, J. Mater. Chem. 27 (2012) 23136.
[29] T.X. Wang, Y.G. Li, H.R. Liu, H. Li, S.-X. Chen, Mater. Lett. 124 (2014) 148.
[30] S. Sarkar, B. Das, P.R. Midya, G.C. Das, K.K. Chattopadhyay, Mater. Lett. 152 (2015) 155.
[31] P. Du, J. Schneider, P. Jarosz, R. Eisenberg, J. Am. Chem. Soc. 128 (2006) 7726–7727.
[32] P. Du, K. Knowles, R. Eisenberg, J. Am. Chem. Soc. 130 (2008) 12576–12577.
[33] Z. Yan, X. Yu, Y. Zhang, H. Jia, Z. Sun, P. Du, Appl. Catal. B 160-161 (2014) 173–178.
[34] R. Abe, K. Hara, K. Sayama, K. Domen, H. Arakawa, J. Photochem. Photobiol. A 137 (2000) 63–69.
[35] K. Kimura, T. Miwa, M. Imamura, Bull. Chem. Soc. Jpn. 43 (1970) 1329–1336.
[36] X. Zhang, Z. Jin, Y. Li, S. Li, G. Lu, J. Colloid Interface Sci. 333 (2009) 285–293.
[37] M. Yin, S. Ma, C. Wu, Y. Fan, RSC Adv. 5 (2015) 1852–1858.
[38] X. Chen, S. Shen, L. Guo, S.S. Mao, Chem. Rev. 110 (2010) 6503–6570.
[39] S.K. Choi, S. Kim, J. Ryu, S.K. Lim, H. Park, Photochem. Photobiol. Sci. 11 (2012) 1437.
[40] X. Yu, X. An, A. Genç, M. Ibáñez, J. Arbiol, Y. Zhang, A. Cabot, J. Phys. Chem. C 119 (2015) 21882–21888.
[41] Z. Wu, J.B. Neaton, J.C. Grossman, Nano Lett. 9 (2009) 2418–2422.
[42] V. Thavasi, G. Singha, S. Ramakrishna, Energy Environ. Sci. 1 (2008) 205–221.
[43] T.J. Macdonald, D.D. Tune, M.R. Dewi, C.T. Gibson, J.G. Shapter, T. Nann, ChemSusChem 8 (2015) 3396.